Renewable Energy 199 (2022) 1105–1115

Contents lists available at ScienceDirect

Renewable Energy

journal homepage: www.elsevier.com/locate/renene

City-wide monitoring and contributing factors to shallow subsurface temperature variability in Nanjing, China

Tiansheng Zhang [a], Chun Liu [a,*], Peter Bayer [b], Liwei Zhang [a], Xulong Gong [c], Kai Gu [a], Bin Shi [a,**]

[a] School of Earth Sciences and Engineering, Nanjing University, Nanjing, China
[b] Department of Applied Geology, Martin Luther University of Halle-Wittenberg, Halle, Germany
[c] Key Laboratory of Earth Fissures Geological Disaster, Ministry of Natural Resources (Geological Survey of Jiangsu Province), Nanjing, China

ARTICLE INFO

Keywords:
Shallow geothermal energy
Geothermal monitoring
Subsurface urban heat island

ABSTRACT

Shallow temperatures down to a depth of 100 m were measured over one year in 19 closed boreholes located in Nanjing, China, to reveal the conditions and factors influencing the subsurface thermal regime. A monitoring concept with distributed temperature sensing, fiber Bragg grating-based sensor, and a type of Resistance Temperature Detectors, is implemented, providing spatial distribution characteristics of subsurface temperatures. The results show that temperatures near the surface are most dynamic, influenced by the air temperature. The temperature remains stable at the depth of 10–20 m. The mean transition temperature is 18.1 °C. Borehole measurements are interpolated by using satellite images and surface temperature records to obtain large-scale surface temperature distributions and temporal variations of subsurface temperature. Geological and hydrological conditions are primary factors by affecting subsurface upward heat flux and heat loss. Urban land cover change and enhanced heat release from urbanization contribute to a subsurface urban heat island with intensities of 1.0–4.4 °C. The altered subsurface thermal regime is of primary concern for the management of shallow geothermal energy use. The monitoring concept in this study can provide spatially-temporally continuous profiles of subsurface temperature and become a reference for city-wide geothermal monitoring in other urban areas.

1. Introduction

Shallow geothermal energy (SGE), also called low-enthalpy geothermal energy, is the energy stored in the upper few hundreds of meters of the solid Earth. SGE resources are mostly stable, unaffected by weather conditions, and their utilization has commonly only a minor impact on the environment [1–4]. Besides, SGE technologies such as geothermal heat pumps are small-scale and offer unique opportunities for robust decentralized heat and cold supply, which makes it possible to utilize SGE in many countries [5–7]. Liu [8] estimated that the total available SGE only in China is 2.89×10^{12} kWh, which is enormous and equal to the total energy yield of 3.56×10^{8} t coal.

The environmental advantages and ubiquitous availability of SGE resources have spurred the utilization of geothermal heat pumps and especially of closed-loop systems. These are based on vertical boreholes equipped with single- or double plastic U-tubes, in which a heat carrier fluid is circulated to supply a ground-coupled heat pump. Their numbers are increasing substantially in China at an average annual growth rate of more than 20%. Meanwhile, China has become the worldwide leader in the installation and use of geothermal heat pumps that currently produce around 250 PJ [9]. However, the utilization rate of SGE is still low, with an average value of 2.3% [10], and therefore also in the future augmented growth rates can be expected. As the number of SGE installations increase, new challenges arise in particular in urban regions with a high density of applications. Optimal use of SGE in such environments requires control of potential thermal interference among neighboring systems, integrated management of exploitation and systematic monitoring of evolving subsurface temperature anomalies, chemical and biological consequences [6,11–17]. Understanding the distribution and evolution of subsurface temperature is important for the environmental and economic management of SGE [18–23]. Ideally, proper exploitation of SGE is based on a case-specific geological survey

* Corresponding author.
** Corresponding author.
E-mail addresses: chunliu@nju.edu.cn (C. Liu), shibin@nju.edu.cn (B. Shi).

https://doi.org/10.1016/j.renene.2022.09.044
Received 14 February 2022; Received in revised form 11 August 2022; Accepted 11 September 2022
Available online 14 September 2022

and accompanied by long-term subsurface temperature monitoring. However, thermal changes in the subsurface are invisible from the surface, and in most cases, they evolve unseen over long periods. Urban thermal subsurface management thus requires tailored monitoring strategies.

A straightforward technique for shallow closed-loop geothermal field monitoring is to tie temperature sensors to the outside of the U-type pipes and backfill the borehole together with the pipes [24,25]. However, this is only feasible during installation and needs synchronized early planning of monitoring concept and borehole heat exchanger layout. Moreover, the sensors can be corroded and damaged if they are buried underground for a long time. Another method is to employ fixed or mobile temperature sensors in the U-type pipes filled with the heat carrier fluid, which is mostly water. The obtained temperature data can be accurate when the temperature of the water is equilibrated with the conditions in the ambient rock and soil. It has been demonstrated that this method is practical and can achieve the goal of monitoring shallow geothermal fields regularly and over a long period [26–28].

Previous research on SGE has focused much on techniques of exploitation and utilization of SGE potentials. Many factors can affect the efficiency of SGE systems, such as geological structure, thermal conductivities of rocks and soils, and groundwater flow, which all influence the variability of the subsurface thermal regime. Uplifts and depressions, for example, can change the heat transport in vertical and horizontal directions. Since a formation's bulk thermal conductivity is highest along the direction of a rock layer, the ground temperature of an anticline structure tends to be higher than that of the syncline structure at the same horizontal position [29,30]. Variability of thermal conductivity among different rocks and of water saturation impacts the distribution of ground temperature and observed vertical geothermal gradients [31]. In particular in shallow ground, convective heat transport associated with groundwater flow may even dominate the contribution by conduction. Moreover, the development of urbanization, the transition from bare soil and grass to concrete and tiles, affects the distribution of subsurface temperature in cities, those areas where most of the geothermal applications are applied. Enhanced heat flux into the shallow ground in cities can cause subsurface urban heat islands (SUHI), similar to aboveground urban heat islands (UHI) observed in major cities worldwide. Since rocks and soils have a greater heat capacity and a lower thermal diffusivity than air, the heat energy stored in SUHI is much larger than that in UHI, which improves SGE use potential for the supply of heating systems [32–38]. Typically, SUHIs extend over an entire urbanized area [32,39,40] and they have been detected in many cities all over the world, such as Winnipeg [40], Tokyo [41], Istanbul [42], Cologne [43], Munich [44], Paris [45], Basel [39], Amsterdam [46], and Moscow [47]. Clearly, knowledge of the role and future evolution of a SUHI is essential for long-term sustainable management of the growing number of SGE installations in cities.

Most of the previous studies focused on the subsurface temperatures measured in wells at a depth of 15–30 m below ground level. This is due to the often-limited accessibility of deeper ground through boreholes and wells. Measurements at a greater depth are typically less influenced by recent urbanization and climate change, thus mainly controlled by hydrogeological and geological factors, and are carried out in a few studies. For example, Liu et al. [48] measured the temperature at a depth of 50 m using a thermosyphon in a drilling borehole. Taniguchi et al. [49] used deep groundwater well profiles to examine how deep urbanization yields a deviation of the recorded temperature trends from the expected constant geothermal gradient. These depths were shown to be 97 m in Tokyo, 76 m in Osaka, 65 m in Seoul, and 45 m in Bangkok [18]. Hemmerle et al. [45] obtained the groundwater temperatures at a depth of 150 m from the measurements by local authorities in Paris from the years 1990–2015. But the data are spatially discontinuous, and it is difficult to interpret spatial trends. Ideally, for revealing the influencing factors of urban subsurface temperature, a monitoring approach is needed to provide spatially-temporally continuous profiles of subsurface temperatures. This is especially of interest for understanding SGE utilization and geothermal thermal energy storage potentials.

Geothermal utilization of shallow ground is enjoying unbroken popularity, with growing numbers of installations and continuously refined knowledge of SGE technologies. Also, worldwide, SUHI conditions evolve, but despite all these global trends, integrated urban thermal ground monitoring and tailored assessment of SGE potential evolution are still rare [50–53]. The main objective of this paper is to investigate the influencing factors for the thermal regime in subsurface urban environments based on city-wide geothermal monitoring and to further understand the evolution of SUHIs. This is considered the basis for city-wide spatial urban SGE planning. For this purpose, a concept for monitoring the shallow urban geothermal regime with complementary thermal sensing devices was developed and temperature data over a one-year period in the city of Nanjing were recorded. Additionally, satellite data within a specified period was retrieved to obtain the land surface temperature, and different land use types were distinguished.

In the following, first the study area and the monitoring concept with different complementary devices and data sources are introduced. This delivers a so far not accessible insight in vertical and temporal temperature trends of the subsurface of Nanjing. The in-situ measurements are complemented by land use patterns and above-ground temperatures to identify the major anthropogenic factors and their spatially variable effects, given different geological and hydrogeological conditions. Finally, based on the findings, the viability and potential of the presented monitoring concept is discussed and the conclusions are presented.

2. Monitoring site and methods

2.1. Study area and monitoring sites

Nanjing (32°03′41″N 118°45′49″E), the capital of Jiangsu Province, China, is situated in the lower reaches of the Yangtze River. As an important part of the Yangtze River Delta, Nanjing has a population of over 9 million and it covers an area of about 6500 km^2. Fig. 1 shows the city's average monthly maximum and minimum air temperatures in 2019. It is apparent that it is hottest in August with an average maximum of 32 °C and is coolest in January with an average minimum of 1 °C. In this year, the hottest day with 38 °C was on July 29th, and the lowest temperature of −4 °C was reached on December 30th.

In an earlier study, two stations in Nanjing were built for

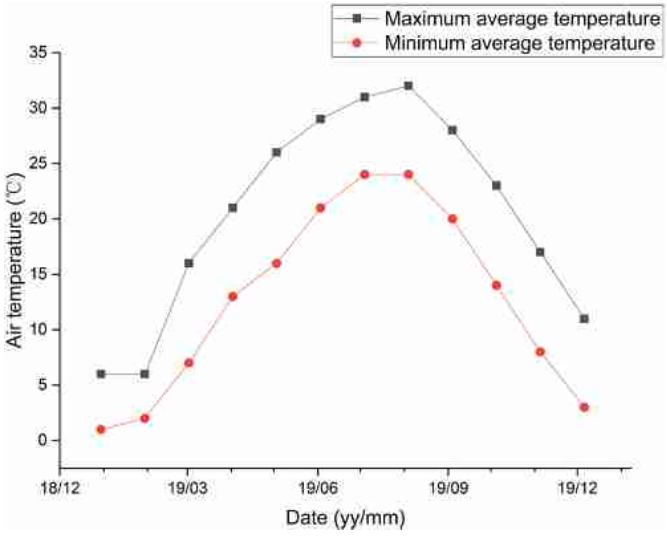

Fig. 1. Trends of average monthly maximum and minimum air temperature in Nanjing, China, for the year 2019 (data from http://www.weather.com.cn/. Accessed: September 13th, 2020).

temperature monitoring of soils at a depth of 0–3m, and these indicated urban soil warming [54]. In 2012, 52 boreholes were drilled in Nanjing by the Geological Survey of Jiangsu Province for deeper subsurface monitoring. However, because of the city expansion and the lack of maintenance, many of these boreholes were covered by pavements, construction sites, or vegetation. For a detailed investigation of the ground thermal evolution over a full year, 19 of these boreholes could be selected in 2018. Their locations and depths are given in Fig. 2 and Table 1, respectively. Most of these boreholes have a depth of 80–100 m, but some boreholes reach only about 70 m. As shown in Fig. 3, a borehole contains two built-in HDPE U-type pipes which are suited to install temperature sensors. Each borehole is covered by a 5 cm thick concrete plate to protect the inner structure from damage. These installations thus are similar to non-backfilled borehole heat exchangers used in closed-loop ground source heat pump systems. However, the major difference in this study is that they are not used for heat supply but exclusively for subsurface urban temperature monitoring. To our knowledge, there does not exist any similar observation network elsewhere. A major advantage of the tube-based monitoring network is that the recorded temperature profiles are independent of the occurrence of groundwater. In fact, most SUHI studies rely on temperature logging in groundwater wells and thus are restricted to aquifers. In Nanjing, additionally to vertical temperature profiling, at five sites in the city center land surface temperatures were recorded by Miniature Thermochron iButton dataloggers.

2.2. Monitoring concept

For resolving the entire depth of boreholes, distributed temperature sensing (DTS) was used at all 19 stations. Based on the temperature characteristics of the scattered light in the fiber, DTS can detect temperature changes and obtain the temperature variability along the fiber [55,56]. The precision of the devices used here is about 0.3 °C. To control, maintain and validate the precision of the temperature data obtained by DTS, Pt100 and fiber Bragg grating (FBG)-based temperature sensors were used. The Pt100 sensor, a type of Platinum resistance thermometer, has a precision of 0.1 °C. It was used to measure temperature at multiple depths ranging from surface to 30 m below, but not deeper due to the limit of maximum cable length. In comparison, an FBG-based sensor's accuracy can theoretically reach 0.05 °C, while its practical accuracy is considered worse, because it is prone to damages during application and thus become inaccurate. FBG-based sensors were installed to measure temperature at depths of 2 m, 5 m, 10 m, 20 m, 40 m, 60 m, and 80 m in two boreholes as a supplement to the Pt100

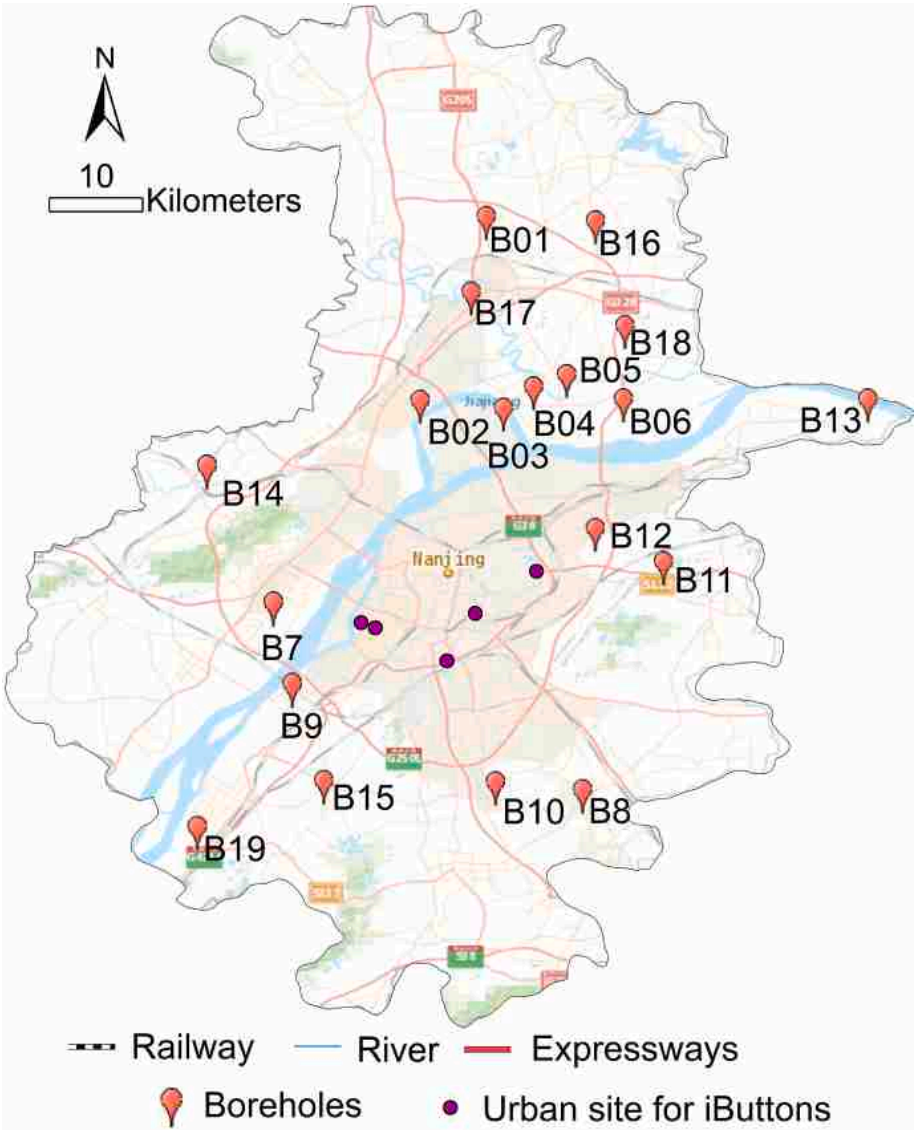

Fig. 2. Locations of 19 boreholes and five land surface measurement urban stations with iButtons in Nanjing.

Table 1
Temperature of the transition zone in all boreholes B1–B19.

Borehole number	Geographical location	Depth (m)	Mean temperature of the transition zone (°C)	Geothermal gradient (°C/100m)
B1	32°22′41.3″N 118°50′02.0″E	90	18.1	1.6
B2	32°12′03.3″N 118°46′13.5″E	96	18.2	1.8
B3	32°11′34.3″N 118°51′01.0″E	92	18.2	2.4
B4	32°12′54.4″N 118°52′49.9″E	96	17.8	2.7
B5	32°13′34.9″N 118°54′44.8″E	93	18.2	2.6
B6	32°12′14.3″N 118°58′02.7″E	95	17.9	2.3
B7	32°00′24.0″N 118°37′35.9″E	95	17.8	1.2
B8	31°49′38.0″N 118°55′33.6″E	75	18.4	1.0
B9	31°55′30.8″N 118°38′46.3″E	77	18.5	1.5
B10	31°50′02.5″N 118°50′30.3″E	95	18.3	1.4
B11	32°02′44.5″N 119°00′22.4″E	80	18.3	6.5
B12	32°04′39.0″N 118°56′18.6″E	95	16.9	1.0
B13	32°12′02.8″N 119°12′10.2″E	90	17.3	2.8
B14	32°08′16.5″N 118°33′54.1″E	75	17.7	0.2
B15	31°50′03.2″N 118°40′41.3″E	67	17.4	2.1
B16	32°22′24.2″N 118°56′26.1″E	100	17.9	1.0
B17	32°18′22.1″N 118°49′12.4″E	93	18.0	1.0
B18	32°16′21.1″N 118°58′05.4″E	100	17.4	3.0
B19	31°47′21.3″N 118°33′16.5″E	95	17.7	1.6

sensors. The DTS temperature data presented in this paper is validated by the Pt100 and FBG-based sensors.

The configuration of the three different temperature monitoring devices in a borehole is shown in Fig. 3. FBG sensors and DTS fiber were inserted in the U-pipes. Aboveground FBG interrogator and DTS extension module were used to interpret and record the data. The temperature data in 19 boreholes (B1–B19) were recorded every season in 2019, including January, April, July, and November. Note that the temperature data in April in some boreholes (B15–B19) are lost and thus not presented. Furthermore, in B4–B10, the temperature was also recorded in January 2020.

The insight from the borehole measurements was complemented by utilizing further information sources: to better understand the effects of the urbanization on the shallow geothermal regime, a satellite image taken in September 2019 by the Landsat 8 satellite was used to get the surface temperature of Nanjing. Besides, to further inspect the shallow subsurface temperature in the downtown area of the city, iButtons were implemented at a very shallow depth of 5 cm in 5 urban sites and near the 19 boreholes from November 2019 to March 2020, and they were configured to record temperatures at time steps of 1 h.

3. Results

3.1. Vertical and temporal temperature trends in boreholes

Fig. 4 depicts temperature-depth profiles of boreholes with full coverage of all four seasons. In these 14 monitored boreholes, 10 boreholes are selected as representatives of the general distribution of

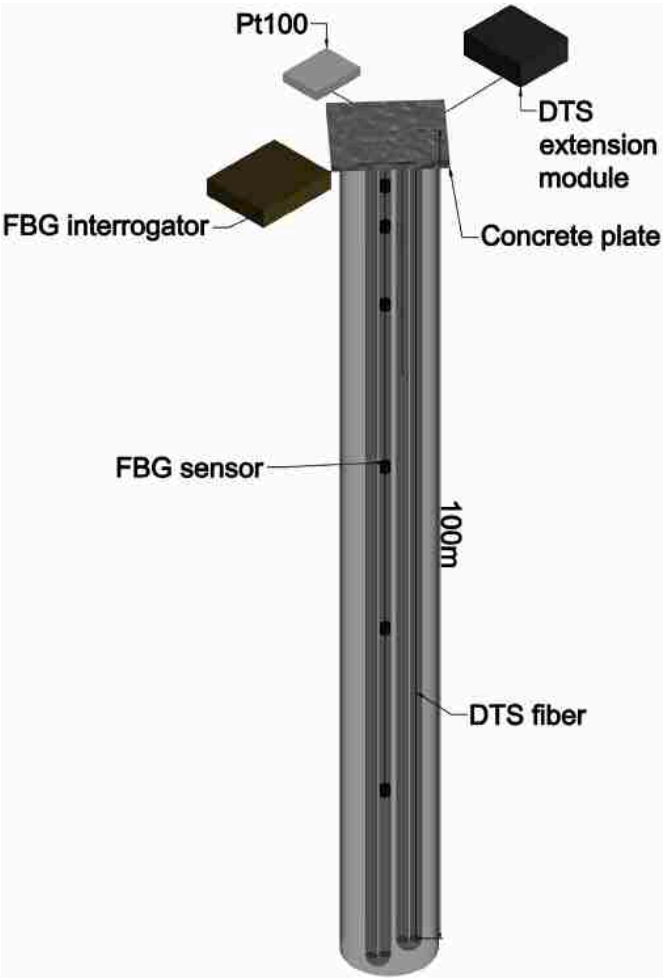

Fig. 3. Sketch illustrating the configuration of the borehole thermal sensing devices.

subsurface temperature in Nanjing. And other 4 boreholes are sorted as abnormal for their temperature profiles are not consistent with the general picture. It can be seen that the temperature trends in the upper part vary depending on the season. In spring and summer (Fig. 4a–b), with the depth along the borehole, the temperature first strongly decreases and then increases below around 15 m, and the overall temperature in the summer (Fig. 4b) is higher. In autumn and winter (Fig. 4c–d), it is the opposite: the temperature first increases and decreases below 15 m, and the overall temperature in the winter is lower.

Fig. 5 presents the temperature of B4–B10 at a depth of 0–20 m from January 2019 to January 2020. Note that, due to system outage, the temperature of B6 in January 2020 was not recorded, so the data of B6 is not presented in Fig. 5. Near the surface (0–5 m in depth), the range of the ground temperature variation is largest. The ground temperature can reach over 30 °C in the summer and a minimum of about 8 °C in the winter following the air temperature shown in Fig. 1, the temperature at the depth of 2 m follows a similar pattern as the air temperature. At the depth of 4 m, 6 m and 8 m, the temperature curves have similar shapes, but the seasonality is shifted with annual maximum and minimum temperatures in fall and spring. Also, as expected, variations are highly site-specific and increasingly dampened with depth and, for the study case, they cannot be clearly detected anymore beyond a depth of 15 m. The top 15 m thus can be roughly distinguished as the seasonal zone [57].

As shown in Fig. 5, within a depth of around 15–20 m, the temperature remains relatively stable in all seasons, and variations are in the range of the accuracy of the sensing devices. In this transition zone of

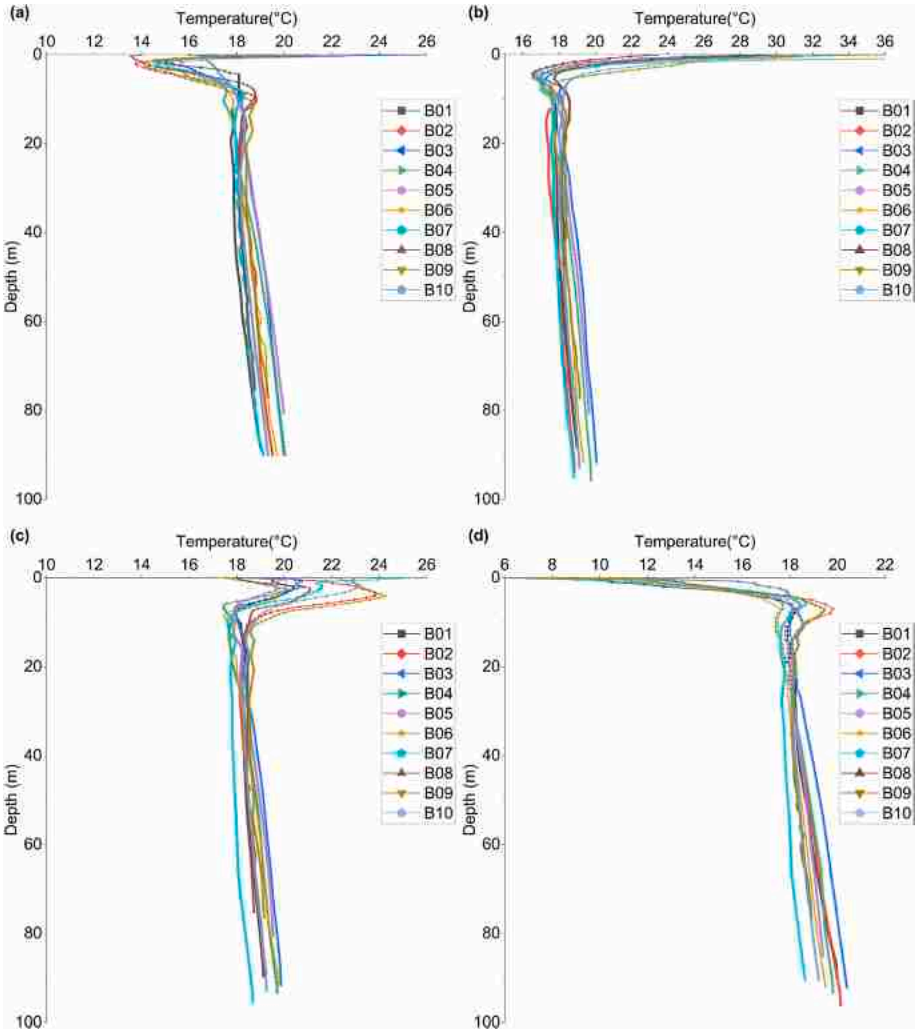

Fig. 4. The ground temperature-depth profiles of 10 boreholes measured in (a) April, (b) July, (c) November, and (d) January 2019 (Data repository available: http://doi.org/10.17632/mkbtbbfyht.1).

subsurface temperature, the seasonal influence thus is hard to be detected. In some studies, the transition zone is also called the constant zone or the normal temperature layer, as the temperatures appear unchanged during the seasons [10,58]. Table 1 presents the mean DTS temperature of the transition zone in the boreholes. The mean temperature of this zone in all 19 boreholes is 18.1 °C.

The temperature gradually increases in the steady zone below the depth of 20 m at a geothermal gradient as listed in Table 1. The computed values span a considerable range between 0.2 and 6.5°C/100 m. Considering the comparable trends of B1–B10, these are taken to derive an average, normal profile of transition and steady zone as reference. The reference, normal profile starts from the depth of 15m because the transition and steady zone is below 15m, and it is shown in Fig. 6 as the black square-dot line. The profiles of B11–B14 are not consistent with the general picture below 15 m. For example, the transition zone in B11 (Fig. 6a) is not obvious and here we find by far the highest geothermal gradient. In contrast, B12 reveals much lower temperatures in the transition and the steady zone (Fig. 6b). Here exist remarkable differences in the repeated profiles at greater depth, and especially the January temperature trends are higher at depths of more than 30 m. Another borehole with unique conditions is B13 (Fig. 6c), with the temperature of the transition zone reaching only 17.3 °C, and the temperature fluctuates in the depth range of around 10–55 m. Finally, at B14 (Fig. 6d), the geothermal gradient is minimal at only 0.2 °C/100 m, and it even is locally negative at the depth of 20 m. The reasons leading to different temperature profiles in B10–B14 are mostly related to geological structure and hydrogeological conditions and will be discussed below.

3.2. Land surface and shallow subsurface temperatures

Based on the satellite image from September 13th, 2019, the land surface temperature shown in Fig. 7a was retrieved based on the multi-channel method [59]. Fig. 7b illustrates the urban land use of Nanjing in 2020. Comparing these two images, it can be concluded that the land surface temperature is highly related to the urban land use in this city. High land surface temperatures mostly appear in the center of the city where the land uses are categorized as residential or industrial areas. Several sites with high temperatures away from the center are associated with industrial zones and larger infrastructures, such as the airport. In contrast, low-temperature regions mostly coincide with green land, agricultural regions, and water bodies.

Fig. 8 depicts shallow subsurface temperatures from November 2019 to March 2020 in the Nanjing region. The time series representing urban areas is the mean of the temperature data obtained by the iButtons set in the city center (Fig. 2), and those in rural areas are the mean temperature obtained by the iButtons set beside boreholes. The subsurface temperature diurnal variations in urban areas are larger than those in rural areas. The temperature differences between urban- and rural areas are also presented in Fig. 8. In November 2019 and March 2020, the

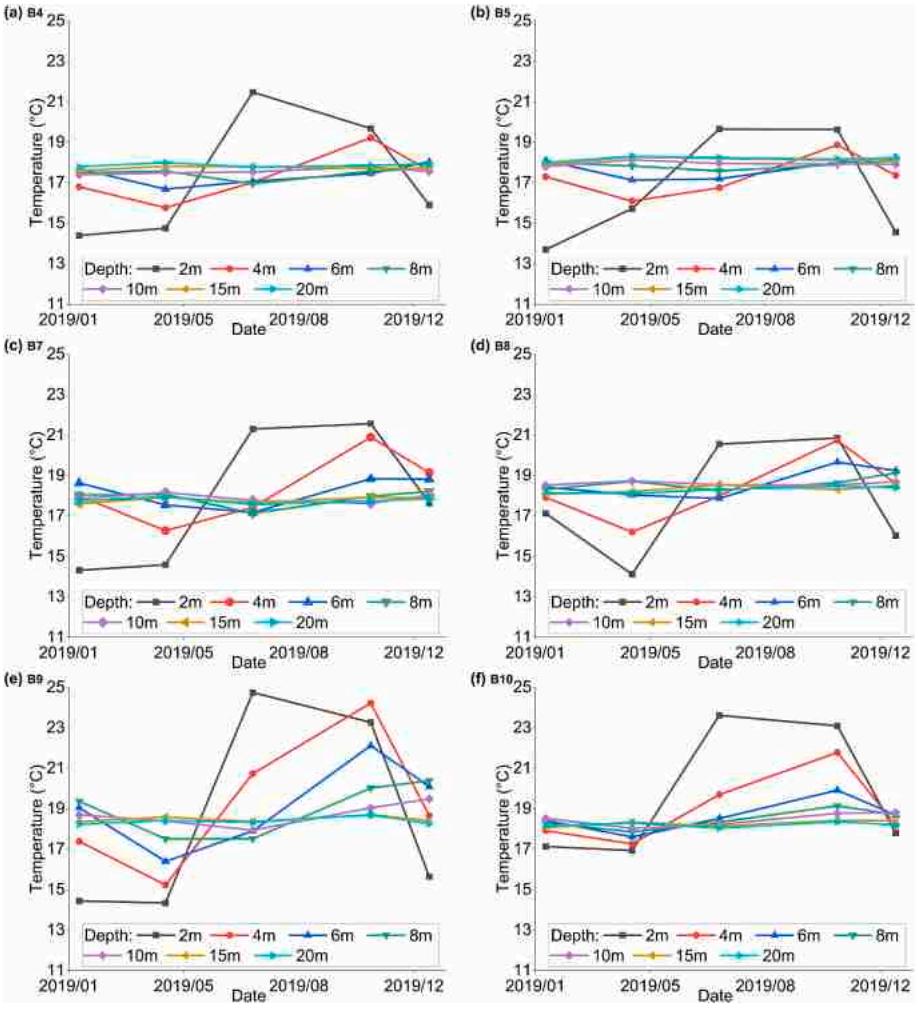

Fig. 5. The temperature of B4–B10 at a depth of 0–20 m from January 2019 to January 2020.

temperatures in urban areas are higher than those in rural areas. However, during the cold season, from December 2019 to February 2020, the temperatures in both areas are close and sometimes the temperatures representing urbanized areas are even lower.

4. Discussion

There exist different sources that supply the energy of the shallow geothermal regime, the Earth's internal heat mainly provided by conduction, as well as solar radiation that contributes from the atmosphere and which represents the dominant heat source for replenishment during imbalanced operation of shallow closed-loop geothermal heat pumps [23]. The availability of SGE resources and the shallow subsurface thermal regime is not only affected by these two factors, but also related to the geological structure, hydrogeological conditions, physical properties of rock and soil, land cover and urbanization. Especially direct anthropogenic heat release and accelerated heat flux from urbanized areas have been reported as a locally relevant aspect [39,40,60,61]. Therefore, the distribution of ground temperature varies in different areas, and geothermal anomalies may occur locally. For the city of Nanjing, the superpositioning of different heat sources manifests in the recorded borehole profiles. In the following, the interpretation of the thermal conditions found throughout the city is discussed, and this discussion is supported by the complementary measurements at the ground and land surface.

As shown in Fig. 4, the temperature from surface to below 15m vary seasonally. This variability is as expected and mostly caused by the thermal coupling between atmospheric seasonal changes and the ground thermal regime. Below the depth of 15 m, the temperatures mostly remain stable. For B1–B10, despite different locations and natural conditions, their conditions are stable throughout the year so that their temperature variations are slight, and trends are similar. So, a "normal" temperature-depth profile can be drawn as average from these boreholes and shown in Fig. 6 as a square-dot line. In this normal profile, the temperature of the transition zone is 18.4 °C, and the overall geothermal gradient is about 2.0 °C/100 m. However, in B11–B14, different temperature trends are observed, obviously influenced by their special local conditions.

4.1. Influence of geological structure and hydrogeological conditions

Geological and associated hydrogeological heterogeneity on different scales strongly controls the variability of the shallow thermal regime. The geological structure determines conductive heat flow variability by facies-specific thermal properties, and the heterogeneous permeability distribution is fundamental for spatially variable advective heat transport driven by groundwater. On a regional km-scale, larger geological structures such as folds and fault zones may have a strong influence on the observed distribution of subsurface temperature [62]. This is also visible for our study case: Borehole B11 (Fig. 6a) is located in the Tangshan area where faults are developed above the Tangshan anticline, mainly ring faults and northeast faults. Previous surveys have shown that the groundwater temperature in the Tangshan area is much higher than those in the surrounding [63]. The reason for the high

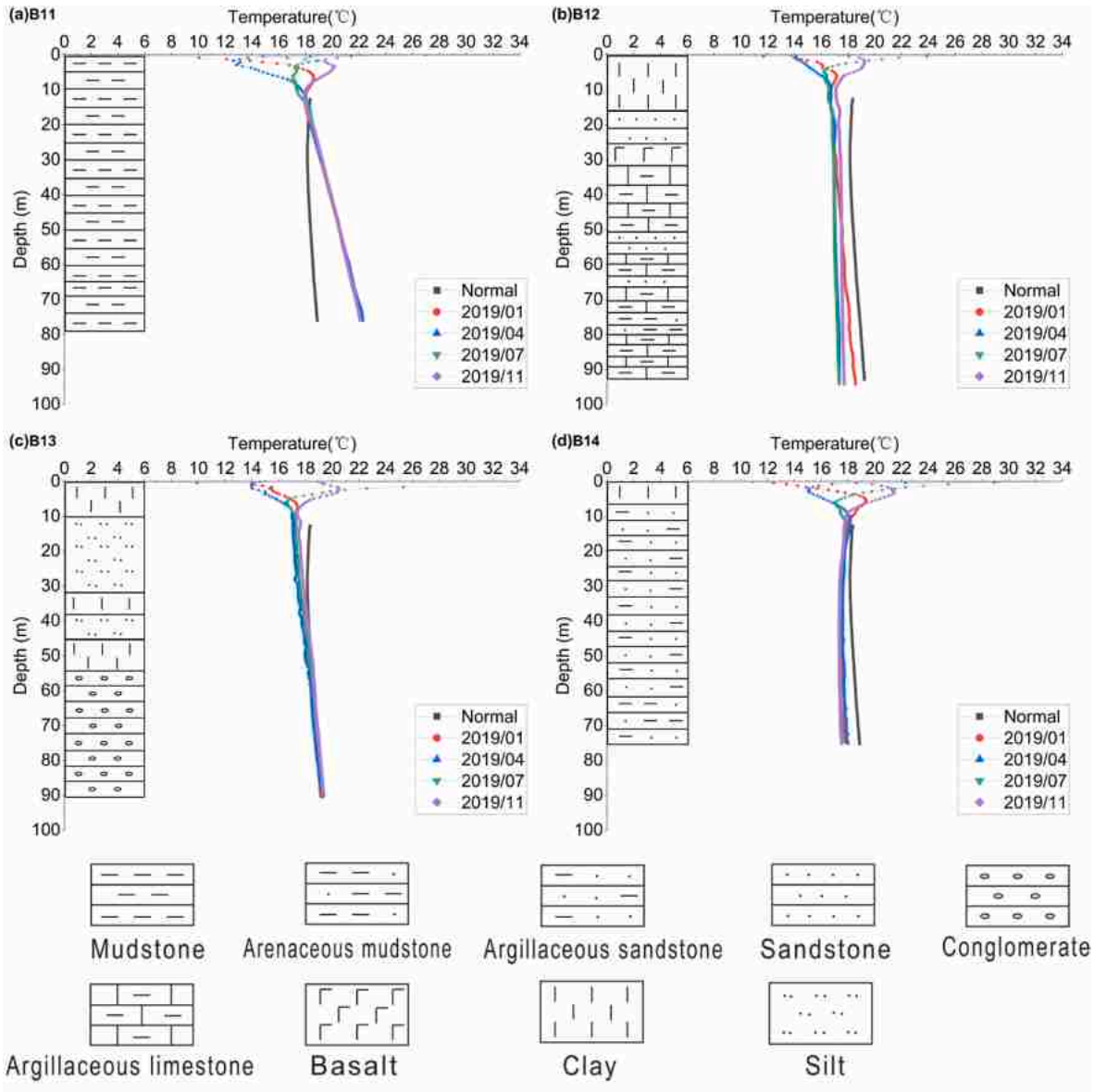

Fig. 6. Ground temperature-depth profiles and lithologies of boreholes B11–B14.

geothermal gradient anomaly in B11 is the accelerated upward heat flux at the fault zone. Here the rock mass is fragmented and, additionally, in the mudstone-dominated formation, karst caves and fissures exist. This yields a weakened zone of enhanced permeability and thus regional vertical groundwater flow focusing. In the fault intersection zone this manifests by underground hydrothermal enrichment, and some hot springs form at the surface. Accordingly, at this borehole, the highest geothermal gradient is observed.

Borehole B12 is located in the southeast of Mount Ling, where also karst has developed in mainly argillaceous limestone below 30 m (Fig. 6b). There exists a considerable uncertainty in the groundwater flow regime in this area, influenced by a high heterogeneity of limestone matrix permeability, karst pores and channels. In contrast to B11, however, the geothermal gradient is lower than the “normal” gradient. This may indicate enhanced vertical water circulation and infiltration with a pronounced downward groundwater flow component. As a result, the profiles vary throughout the year even at a great depth of 90 m.

B13 is situated in the floodplain of the Yangtze River overlain with thick Quaternary sediments. As shown in Fig. 6c, the lithology of B13 from the surface to a depth of 55 m is characterized by multiple layers of clay and silt, and below 55 m by moderately weathered conglomerate. The vertical trend of ground temperature in B13 deviates from the normal profile mainly within the silty layer, which is interpreted by enhanced advection in the young floodplain sediments above the isolating clay formation. Thus, the ground temperature of B13 fluctuates here more and the temperature of the transition zone is lower than that of the other boreholes.

The area where B14 is located in the floodplain area of the Chuhe River, covered with an about 10 m thick overfill and clay. Fig. 6d shows that the main lithology of B14 is argillaceous sandstone with a thin stratum of arenaceous mudstone. The temperature below 20 m stays nearly stable down to 75 m close to the temperature in the transition zone. Despite the possible fissures developed in it, the sandstone is relatively impermeable, which means that the groundwater has little effect on the ground temperature here. The low geothermal gradient in B14 thus is caused by other effects. As one possibility the heat flux from the deeper crust is lower than usual, but no previous studies indicated that a crustal geothermal anomaly exists here. Another and more probable factor thus may be the thermal property of the investigated sediments here, e.g., a thermal blanket, but for instance, a considerable

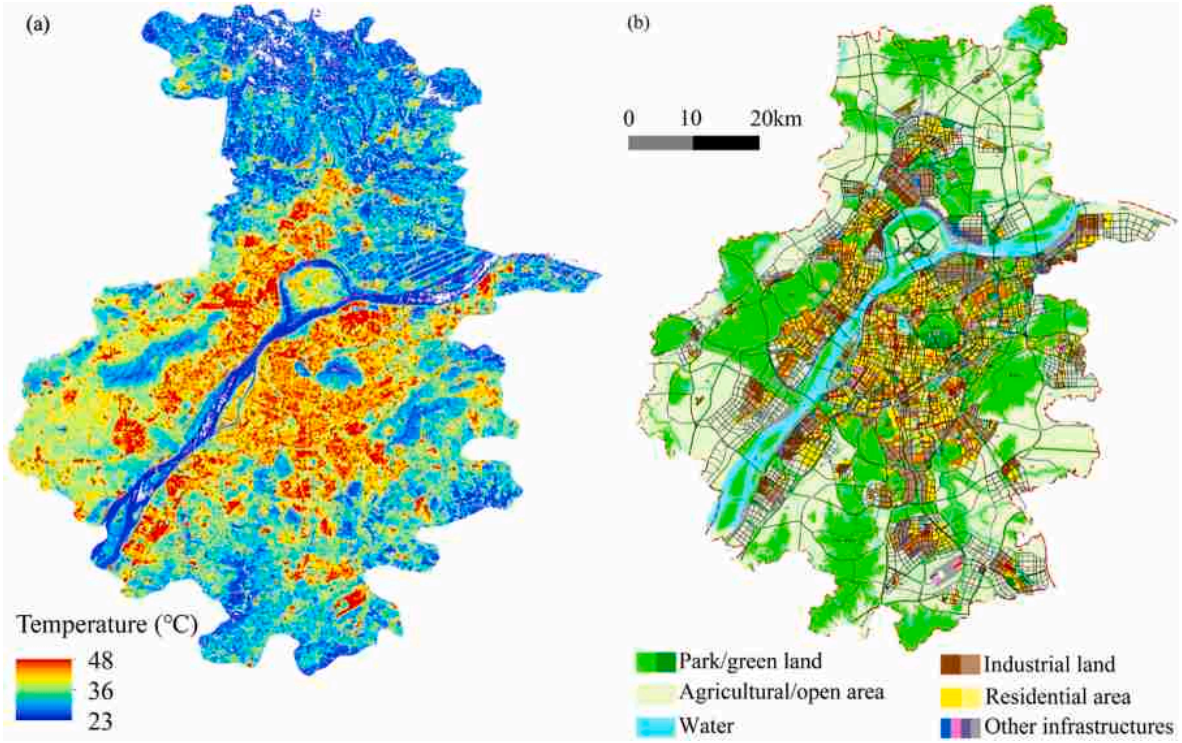

Fig. 7. (a) Land surface temperature retrieved from satellite image in September 2019 (satellite data from: http://www.gscloud.cn. Accessed: November 23rd, 2020); (b) urban land use of Nanjing city in 2020 (from Nanjing Municipal People's Government, http://ghj.nanjing.gov.cn. Accessed: November 23rd, 2020).

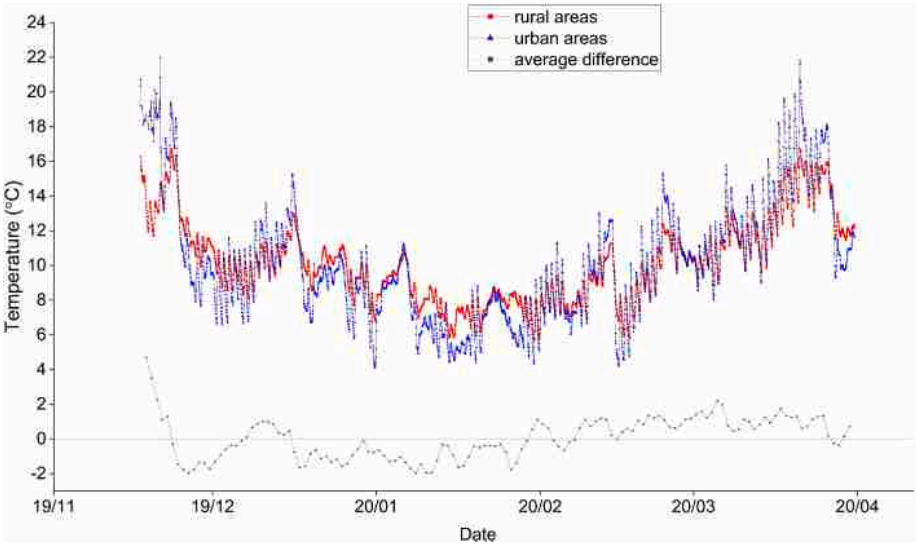

Fig. 8. Temperatures obtained by iButtons from November 2019 to March 2020 in urban- and rural areas of Nanjing.

higher thermal conductivity of the arenaceous mudstone has not been substantiated. Thus, no clear interpretation of the abnormal observation can be derived for this borehole.

4.2. Role of land cover and urbanization

In the transition zone, the mean heat input from the bottom is equal to the mean heat input from the ground surface, and therefore the temperature is stable and unchanged seasonally. However, this zone can change and move responding to long-term, non-seasonal variations. With ongoing global climate warming, the mean air temperature and the heat input from the surface changes, which will rebalance the heat equation in the transition zone and influence the temperature [57]. However, such long-term changes cannot be detected by comparing the repeated logging at single boreholes over one year in this study.

Furthermore, by affecting the conduction of near-surface heat at the ground, the type of land cover can have a strong influence on the shallow subsurface temperature [26,64]. For example, the temperature of the soil covered by concrete and other hard ground is higher than that of bare soil and grassland [65]. Similar to metropolises all over the world, the urbanization in Nanjing is rapid and the type of land use has changed much, indicating that the sealed land expands, and the fraction of agricultural and forest land shrinks down gradually [66]. With the effects of urbanization, bare and green lands have been converted into

pavements and covered by concrete buildings; the release of heat rises due to the population growth and the large-scale use of ground and underground transportations. The results shown in Fig. 7 thus reveal that the surface temperatures in densely built-up areas of Nanjing are higher than those in green lands. The high temperature areas are mostly situated in the downtown, delineating stronger urban heat island intensities towards the city center.

Associated with above-ground urban heat islands, there often exist subsurface urban heat islands (SUHIs), which are not only mirrors of the atmospheric temperatures but reveal greater thermal anomalies in comparison to the natural state, and which represent a much higher enhanced energy density to be used as a reservoir for SGE [33,67]. Ground surface temperatures are influenced by many factors, such as solar radiation and regional weather. Including underground infrastructures, building basements, industrial thermal waste, and underground water extractions, the processes of urbanization change the heat flux at the surface, affect the direction of heat flow and generate extra heat flux into the subsurface. This phenomenon is also shown in Fig. 8, where the subsurface temperature in urban areas is different from that in rural areas. Moreover, the temperature diurnal variation in urban areas is also higher than that in rural areas. This is controlled by the different properties of the land cover and underlying soil. Pavements and concretes preserve less heat than bare soil and grasslands. Another reason is that land covers in urban areas consume less heat for water evaporation since the water flows away rapidly on the sealed surface.

The results from Fig. 8 show that the intensity of the SUHI close to the ground surface in the seasonal zone varies over the year. In spring and fall, the temperature differences can be seen, from 1.0 °C to 2.4 °C, even to 4.4 °C. This observation may suggest that the effects of SUHI are the strongest in summer and the weakest in winter, which is consistent with previous research [61]. While in winter, the differences of shallow subsurface temperatures in rural and urban areas are mostly negative, which means the effects of SUHI decline and an opposite effect even exists. Two possible reasons may be able to explain this observation. First, as shown in Figs. 2 and 7, two urban monitoring stations are close to the Purple Mount and Xuanwu Lake (a relatively cold area in the city center), which may ease the effects of SUHI and reduce the temperature differences. Another possible reason is that sealed lands have a lower buffer capacity. In Fig. 8, the temperature differences in winter fluctuate and are highly related to the cold fronts accompanied by rains and snows, according to local weather history data. It may suggest the temperature in urban areas drops faster within cold fronts and an opposite effect is shown. Besides, there are fluctuations in the temperature differences on a smaller scale. Many reasons can cause those fluctuations, e.g., regional rainfall, human activities in monitoring sites. In this study, only the urban temperature at a depth of 5 cm was recorded by iButtons. However, the depth that the SUHI can influence is much more than 5 cm. The actual influenced depth varies among cities and mainly depends on the degree of urbanization and local microclimate. Some infrastructures, such as subways and underground shopping centers, can reach a depth of dozens of meters, which will change the subsurface temperature to a great extent. Though boreholes profiles reach greater depths, present boreholes still are not representative of urban temperature.

4.3. Evaluation of monitoring approach

In this study, multiple monitoring techniques were applied, including borehole monitoring, iButtons, and satellite images. All of them together serve as a new integrated monitoring concept for shallow geothermal monitoring in cities. For borehole monitoring, DTS, FBG, and Pt100 sensors were applied. Spatially continuous trends of borehole temperature were provided by DTS. FBG and Pt100 sensors were used to monitor temperature at specific points for the calibration of possible errors in DTS. However, FBG implemented in boreholes is liable to be damaged during application and become inaccurate, which may require supporting field tests with FBG during geothermal monitoring. Though the application of FBG was less successful, the borehole monitoring approach of this study can clearly present spatially continuous temperature-depth profiles in boreholes, which addresses the issue of spatially discontinuous data in previous studies [44,45,47,48]. Aside from this, its accuracy can be ±0.3 °C, providing more precise profiles of underground temperatures. Additionally, to obtain land surface temperatures, iButtons were employed to measure temperatures with high accuracy of 0.1 °C and to trace temporal changes at monitoring sites. Satellite data complements the local measurements by providing a snapshot of the large-scale land surface temperature in Nanjing, and it delineates temperature differences among areas. With two elements of monitoring, boreholes and land surface, spatial and temporal distributions of underground temperatures in city-wide areas can be drawn out. Their precision varies depending on the spatial density and frequency of monitoring, which can be adjusted according to the actual demands. The monitoring concept in this study provided city-wide subsurface temperature data with spatial continuity in a depth range of 0–100m. Based on the experience in Nanjing, the whole monitoring concept can be applicable to other areas and cities for large-scale shallow geothermal monitoring.

5. Conclusions

This study is dedicated to developing a subsurface temperature monitoring concept for an expanding metropole such as Nanjing with growing interest in shallow geothermal energy (SGE). As the primary data source, the profiles of 19 closed boreholes were monitored seasonally in 2019. The conclusions of this study are as follows:

(1) A normal mean trend of the subsurface temperature in Nanjing is derived and three zones can be distinguished: from the surface to 15 m below the ground level is the variable zone of the subsurface temperature, where the temperatures seasonally follow the pattern of the air temperature. At a depth of 15 m–20 m is the transition zone, where the temperatures are stable at about 18.1 °C. At 20 m and deeper is the steady zone where the temperature profile delineates the shallow geothermal gradient.
(2) These normal conditions serve as a reference to find special local conditions and for interpretation of the variable influencing factors that lead to special thermal anomalies. It is revealed that the geological structure and hydrogeological conditions play an important role in the distribution of the subsurface temperature. In the area of borehole B11, the geothermal gradient reaches about 6.5 °C/100 m and hot springs form in the area. Here, intersection faults form the heat channels between the surface and the deep crust. The temperature fluctuations observed in B12–B13 are most strongly influenced by groundwater flow. Therefore, knowledge of the regional geological structure and the hydrogeological regime is key for planning optimal utilization of SGE.
(3) The type of land cover has a main impact on the temperature near the surface. Urbanization causes a SUHI and as the expansion of a city continues and the underground constructions become deeper, subsurface heating increases and this offers additional opportunities for SGE to provide heat supply of cities. However, subsurface heat accumulation hampers efficient SGE use for cooling which is of growing interest for a city such as Nanjing.
(4) The monitoring concept in this study can provide a reference for shallow geothermal monitoring on a city scale. With the application of DTS and Pt100, borehole depth-temperature profiles can be obtained with spatially continuity and high accuracy. iButtons measure temperatures at a depth of 5 cm with high accuracy of 0.1 °C and provide temporally continuous profiles at sites. Satellite data provides a snapshot of land surface temperature on a city scale. With borehole and land surface monitoring,

spatial and temporal distributions of subsurface temperatures can be acquired. The new monitoring concept used in this paper can be used in other areas and cities for shallow geothermal monitoring.

The boreholes and monitoring sites cover parts of the Nanjing city, though some regions, such as the center of the city and major infrastructures, are not fully covered. Depending on the future work, more monitoring sites may be added if a more detailed profile of some areas is needed. Furthermore, with the temperature data and detailed geological conditions, numerical simulations of subsurface heat transferring in a certain area can be made and verified, which will better clarify the evolution of SUHIs. It is of great importance to monitor and understand SUHI in the consideration of the rapid development of the economy and urbanization. The result of city-wide monitoring provides a reference for city management of SGE.

CRediT authorship contribution statement

Tiansheng Zhang: Writing – original draft, Visualization, Conceptualization, Investigation, Data curation, Formal analysis. **Chun Liu:** Writing – review & editing, Conceptualization, Project administration, Funding acquisition, Methodology. **Peter Bayer:** Writing – review & editing. **Liwei Zhang:** Investigation, Data curation. **Xulong Gong:** Resources. **Kai Gu:** Writing – review & editing. **Bin Shi:** Supervision.

Declaration of competing interest

The authors declare that they have no known competing financial interests or personal relationships that could have appeared to influence the work reported in this paper.

Acknowledgments

This study was supported and funded by the National Natural Science Foundation of China (Grant No. 41761134089, 41977218, 41977217), and Six talent peaks project of Jiangsu Province (Grant No. RJFW-003). The collaborative study was also supported by the German research foundation DFG (grant No. BA2850/3-1). Basic geological data of the boreholes are provided by the Geological Survey of Jiangsu Province.

References

[1] D. Saner, R. Juraske, M. Kuebert, P. Blum, S. Hellweg, P. Bayer, Is it only CO2 that matters? A life cycle perspective on shallow geothermal systems, Renew. Sustain. Energy Rev. 14 (7) (2010) 1798–1813, https://doi.org/10.1016/j.rser.2010.04.002.

[2] P. Bayer, D. Saner, S. Bolay, L. Rybach, P. Blum, Greenhouse gas emission savings of ground source heat pump systems in Europe: a review, Renew. Sustain. Energy Rev. 16 (2) (2012) 1256–1267, https://doi.org/10.1016/j.rser.2011.09.027.

[3] R.R. Zhang, G.L. Wang, X.X. Shen, J.F. Wang, X.F. Tan, S.T. Feng, J.L. Hong, Is geothermal heating environmentally superior than coal fired heating in China? Renew. Sustain. Energy Rev. 131 (2020), 110014 https://doi.org/10.1016/j.rser.2020.110014.

[4] J. Luo, W. Xue, H.B. Shao, Thermo-economic comparison of coal-fired boiler-based and groundwater-heat-pump based heating and cooling solution - a case study on a greenhouse in Hubei, China, Energy Build. 223 (2020), 110214, https://doi.org/10.1016/j.enbuild.2020.110214.

[5] M. Alcaraz, A. Garcia-Gil, E. Vazquez-Sune, V. Velasco, Advection and dispersion heat transport mechanisms in the quantification of shallow geothermal resources and associated environmental impacts, Sci. Total Environ. 543 (2016) 536–546, https://doi.org/10.1016/j.scitotenv.2015.11.022.

[6] M. Alcaraz, A. García-Gil, E. Vázquez-Suñé, V. Velasco, Use rights markets for shallow geothermal energy management, Appl. Energy 172 (2016) 34–46, https://doi.org/10.1016/j.apenergy.2016.03.071.

[7] L. Rybach, Geothermal heat pumps, Encyclopedia of Solid Earth Geophysics (2020) 411–414, https://doi.org/10.1007/978-90-481-8702-7.

[8] Y.P. Liu, Analysis of low carbon emission efficiency of geothermal resources (in Chinese), Hydrogeol. Eng. Geol. 40 (6) (2013) 134–138, https://doi.org/10.16030/j.cnki.issn.1000-3665.2013.06.013.

[9] J.W. Lund, A.N. Toth, Direct utilization of geothermal energy 2020 worldwide review, Geothermics 90 (2021), 101915, https://doi.org/10.1016/j.geothermics.2020.101915.

[10] Y.S. Xu, X.W. Wang, S.L. Shen, A.N. Zhou, Distribution characteristics and utilization of shallow geothermal energy in China, Energy Build. 229 (2020), https://doi.org/10.1016/j.enbuild.2020.110479.

[11] M.L. Fasci, A. Lazzarotto, J. Acuna, J. Claesson, Analysis of the thermal interference between ground source heat pump systems in dense neighborhoods, Sci Technol Built En 25 (8) (2019) 1069–1080, https://doi.org/10.1080/23744731.2019.1648130.

[12] S. Haehnlein, P. Bayer, P. Blum, International legal status of the use of shallow geothermal energy, Renew. Sustain. Energy Rev. 14 (9) (2010) 2611–2625, https://doi.org/10.1016/j.rser.2010.07.069.

[13] A. García-Gil, G. Goetzl, M.R. Kłonowski, S. Borovic, D.P. Boon, C. Abesser, M. Janza, I. Herms, E. Petitclerc, M. Erlström, J. Holecek, T. Hunter, V. P. Vandeweijer, R. Cernak, M. Mejías Moreno, J. Epting, Governance of shallow geothermal energy resources, Energy Pol. 138 (2020), https://doi.org/10.1016/j.enpol.2020.111283.

[14] X.Y. Li, T.Y. Li, D.Q. Qu, J.W. Yu, A new solution for thermal interference of vertical U-tube ground heat exchanger for cold area in China, Geothermics 65 (2017) 72–80, https://doi.org/10.1016/j.geothermics.2016.08.002.

[15] A. Walch, N. Mohajeri, A. Gudmundsson, J.-L. Scartezzini, Quantifying the technical geothermal potential from shallow borehole heat exchangers at regional scale, Renew. Energy 165 (2021) 369–380, https://doi.org/10.1016/j.renene.2020.11.019.

[16] G. Attard, P. Bayer, Y. Rossier, P. Blum, L. Eisenlohr, A novel concept for managing thermal interference between geothermal systems in cities, Renew. Energy 145 (2020) 914–924, https://doi.org/10.1016/j.renene.2019.06.095.

[17] J. Becher, C. Englisch, C. Griebler, P. Bayer, Groundwater fauna downtown – drivers, impacts and implications for subsurface ecosystems in urban areas, J. Contam. Hydrol. 248 (2022), 104021, https://doi.org/10.1016/j.jconhyd.2022.104021.

[18] T. Vienken, M. Kreck, P. Dietrich, Monitoring the impact of intensive shallow geothermal energy use on groundwater temperatures in a residential neighborhood, Geoth. Energy 7 (1) (2019), https://doi.org/10.1186/s40517-019-0123-x.

[19] C. Abesser, R.A. Schincariol, J. Raymond, A. Garcia-Gil, R. Drysdale, A. Piatek, N. Giordano, N. Jaziri, J. Molson, Case studies of geothermal system response to perturbations in groundwater flow and thermal regimes, Ground Water (2021), https://doi.org/10.1111/gwat.13086.

[20] B.Y. Li, M. Zheng, M. Shahrestani, S.X. Zhang, Driving factors of the thermal efficiency of ground source heat pump systems with vertical boreholes in Chongqing by experiments, J. Build. Eng. 28 (2020), 101049, https://doi.org/10.1016/j.jobe.2019.101049.

[21] B.Q. Tian, Y.L. Kong, Y.L. Gong, C.T. Ye, Z.H. Pang, J.Y. Wang, D.D. Zhang, An improved volumetric method of geothermal resources assessment for shallow ground combining geophysical data, Renew. Energy 145 (2020) 2306–2315, https://doi.org/10.1016/j.renene.2019.08.005.

[22] M.A. Rey-Ronco, M.P. Castro-Garcia, G. Marcos-Robredo, T. Alonso-Sanchez, Study of shallow subsoil temperature and its relationship to thermal diffusivity, Geothermics 86 (2020), https://doi.org/10.1016/j.geothermics.2020.101821.

[23] J.A. Rivera, P. Blum, P. Bayer, Ground energy balance for borehole heat exchangers: vertical fluxes, groundwater and storage, Renew. Energy 83 (2015) 1341–1351, https://doi.org/10.1016/j.renene.2015.05.051.

[24] Y.C. Guo, Jia Zheng, Yu Yuan, Zhe Wang, Zi Long Jia, Introduction to design and implementation of monitoring system for the buried pipe of ground-source heat pump system (in Chinese), Urban Geology 9 (Z1) (2014) 85–88.

[25] L. Rybach, W.J. Eugster, Sustainability aspects of geothermal heat pump operation, with experience from Switzerland, Geothermics 39 (4) (2010) 365–369, https://doi.org/10.1016/j.geothermics.2010.08.002.

[26] P. Bayer, J.A. Rivera, D. Schweizer, U. Schaerli, P. Blum, L. Rybach, Extracting past atmospheric warming and urban heating effects from borehole temperature profiles, Geothermics 64 (2016) 289–299, https://doi.org/10.1016/j.geothermics.2016.06.011.

[27] S. Schüppler, R. Zorn, H. Steger, P. Blum, Uncertainty analysis of wireless temperature measurement (WTM) in borehole heat exchangers, Geothermics 90 (2021), https://doi.org/10.1016/j.geothermics.2020.102019.

[28] N. Aranzabal, J. Martos, H. Steger, P. Blum, J. Soret, Temperature measurements along a vertical borehole heat exchanger: a method comparison, Renew. Energy 143 (2019) 1247–1258, https://doi.org/10.1016/j.renene.2019.05.092.

[29] W.S. Wei, G.S. Zheng, Y.B. Luan, Characteristics and influencing factors of the shallow geothermal field in Beijing plain area (in Chinese), Chin. Geol. 37 (6) (2010) 1733–1739, https://doi.org/10.3969/j.issn.1000-3657.2010.06.019.

[30] L.P. Xiong, W.A. Gao, Characteristics of geotherm in uplift and depression (in Chinese), Acta Geophysica Sinica. 25 (5) (1982) 448–456.

[31] Z.X. Li, J. Gao, W.F. Li, C.L. Liu, Y.S. Ma, The characteristics of geothermal field and controlling factors in Qaidam Basin, Northwest China (in Chinese), Earth Sci. Front. 23 (5) (2016) 23–32, https://doi.org/10.13745/j.esf.2016.05.003.

[32] K. Menberg, P. Blum, A. Schaffitel, P. Bayer, Long-term rvolution of anthropogenic heat fuxes into a subsurface urban heat island, Environ. Sci. Technol. 47 (17) (2013) 9747–9755, https://doi.org/10.1021/es401546u.

[33] K. Zhu, P. Blum, G. Ferguson, K.-D. Balke, P. Bayer, The geothermal potential of urban heat islands, Environ. Res. Lett. 5 (4) (2010), https://doi.org/10.1088/1748-9326/5/4/044002.

[34] P. Bayer, G. Attard, P. Blum, K. Menberg, The geothermal potential of cities, Renew. Sustain. Energy Rev. 106 (2019) 17–30, https://doi.org/10.1016/j.rser.2019.02.019.
[35] S. Baumgärtel, J. Rohn, J. Luo, Experimental study of road deicing by using the urban groundwater under the climatic condition of Nuremberg city, Germany, SN Appl. Sci. 2 (4) (2020) 1–13, https://doi.org/10.1007/s42452-020-2314-2.
[36] A. Bidarmaghz, R. Choudhary, K. Soga, R.L. Terrington, H. Kessler, S. Thorpe, Large-scale urban underground hydro-thermal modelling–A case study of the Royal Borough of Kensington and Chelsea, London, Sci. Total Environ. 700 (2020), 134955, https://doi.org/10.1016/j.scitotenv.2019.134955.
[37] H. Hemmerle, G. Ferguson, P. Blum, P. Bayer, The evolution of the geothermal potential of a subsurface urban heat island, Environ. Res. Lett. 17 (8) (2022), 084018, https://doi.org/10.1088/1748-9326/ac7e60.
[38] S.A. Benz, K. Menberg, P. Bayer, B.L. Kurylyk, Shallow subsurface heat recycling is a sustainable global space heating alternative, Nat. Commun. 13 (1) (2022), https://doi.org/10.1038/s41467-022-31624-6.
[39] J. Epting, P. Huggenberger, Unraveling the heat island effect observed in urban groundwater bodies – definition of a potential natural state, J. Hydrol. 501 (2013) 193–204, https://doi.org/10.1016/j.jhydrol.2013.08.002.
[40] G. Ferguson, A.D. Woodbury, Urban heat island in the subsurface, Geophys. Res. Lett. 34 (23) (2007), https://doi.org/10.1029/2007gl032324.
[41] M. Taniguchi, T. Uemura, Y. Sakura, Effects of urbanization and groundwater flow on subsurface temperature in three megacities in Japan, J. Geophys. Eng. 2 (4) (2005) 320–325, https://doi.org/10.1088/1742-2132/2/4/s04.
[42] T. Yalcin, O. Yetemen, Local warming of groundwaters caused by the urban heat island effect in Istanbul, Turkey, Hydrogeol. J. 17 (5) (2009) 1247–1255, https://doi.org/10.1007/s10040-009-0474-7.
[43] K. Menberg, P. Bayer, K. Zosseder, S. Rumohr, P. Blum, Subsurface urban heat islands in German cities, Sci. Total Environ. 442 (2013) 123–133, https://doi.org/10.1016/j.scitotenv.2012.10.043.
[44] F. Böttcher, K. Zosseder, Thermal influences on groundwater in urban environments – a multivariate statistical analysis of the subsurface heat island effect in Munich, Sci. Total Environ. 810 (2022), 152193, https://doi.org/10.1016/j.scitotenv.2021.152193.
[45] H. Hemmerle, S. Hale, I. Dressel, S.A. Benz, G. Attard, P. Blum, P. Bayer, Estimation of Groundwater Temperatures in Paris, France, Geofluids, 2019, p. 2019, https://doi.org/10.1155/2019/5246307.
[46] P.W. Visser, H. Kooi, V. Bense, E. Boerma, Impacts of progressive urban expansion on subsurface temperatures in the city of Amsterdam (The Netherlands), Hydrogeol. J. 28 (5) (2020) 1755–1772, https://doi.org/10.1007/s10040-020-02150-w.
[47] M.A. Lokoshchenko, I.A. Korneva, Underground urban heat island below Moscow city, Urban Clim. 13 (2015) 1–13, https://doi.org/10.1016/j.uclim.2015.04.002.
[48] H. Liu, X. Wang, L. Zheng, H. Yao, Y. Zhu, Y. Wang, Temperature response and thermal performance analysis of a super-long flexible thermosyphon for shallow geothermal utilization: field test and numerical simulation, Int. J. Heat Mass Tran. 192 (2022), 122915, https://doi.org/10.1016/j.ijheatmasstransfer.2022.122915.
[49] M. Taniguchi, T. Uemura, K. Jago-On, Combined effects of urbanization and global warming on subsurface temperature in four asian cities, Vadose Zone J. 6 (3) (2007) 591–596, https://doi.org/10.2136/vzj2006.0094.
[50] A.M. Patton, G. Farr, D.P. Boon, D.R. James, B. Williams, L. James, R. Kendall, S. Thorpe, G. Harcombe, D.I. Schofield, A. Holden, D. White, Establishing an urban geo-observatory to support sustainable development of shallow subsurface heat recovery and storage, Q. J. Eng. Geol. Hydrogeol. 53 (1) (2020) 49–61, https://doi.org/10.1144/qjegh2019-020.
[51] C. Tissen, K. Menberg, P. Bayer, P. Blum, Meeting the demand: geothermal heat supply rates for an urban quarter in Germany, Geoth. Energy 7 (1) (2019) 9, https://doi.org/10.1186/s40517-019-0125-8.
[52] J. Epting, A. García-Gil, P. Huggenberger, E. Vázquez-Suñe, M.H. Mueller, Development of concepts for the management of thermal resources in urban areas–assessment of transferability from the Basel (Switzerland) and Zaragoza (Spain) case studies, J. Hydrol. 548 (2017) 697–715, https://doi.org/10.1016/j.jhydrol.2017.03.057.
[53] R. Perego, G. Dalla Santa, A. Galgaro, S. Pera, Intensive thermal exploitation from closed and open shallow geothermal systems at urban scale: unmanaged conflicts and potential synergies, Geothermics 103 (2022), 102417.
[54] B. Shi, C.S. Tang, L. Gao, C. Liu, B.J. Wang, Observation and analysis of the urban heat island effect on soil in Nanjing, China, Environ. Earth Sci. 67 (1) (2012) 215–229, https://doi.org/10.1007/s12665-011-1501-2.
[55] Z.P. Song, D. Zhang, H.D. Fang, B. Shi, B. Fei, Fiber optic monitoring of temperature during hydration heat release process of large slab concreting for ship lock (in Chinese), J. Eng. Geol. 22 (2) (2014) 244–249, https://doi.org/10.13544/j.cnki.jeg.2014.02.010.
[56] W.W. Zou, Z.Y. He, K. Hotate, Complete discrimination of strain and temperature using Brillouin frequency shift and birefringence in a polarization-maintaining fiber, Opt Express 17 (3) (2009) 1248–1255, https://doi.org/10.1364/oe.17.001248.
[57] B.L. Kurylyk, D.J. Irvine, V.F. Bense, Theory, tools, and multidisciplinary applications for tracing groundwater fluxes from temperature profiles, Wires Water 6 (1) (2019), e1329, https://doi.org/10.1002/wat2.1329.
[58] W.Z. Cui, S.Y. Zhou, Q.Y. Peng, Underground Thermal Properties Analysis for Ground Source Heat Pump Application, 2015 4th International Conference on Energy and Environmental Protection, 2015, pp. 470–473. Iceep. 2015.
[59] Z.L. Li, B.H. Tang, H. Wu, H. Ren, G. Yan, Z. Wan, I.F. Trigo, J.A. Sobrino, Satellite-derived land surface temperature: current status and perspectives, Rem. Sens. Environ. 131 (2013) 14–37, https://doi.org/10.1016/j.rse.2012.12.008.
[60] C. Tissen, S.A. Benz, K. Menberg, P. Bayer, P. Blum, Groundwater temperature anomalies in central Europe, Environ. Res. Lett. 14 (10) (2019), 104012, https://doi.org/10.1088/1748-9326/ab4240.
[61] C.S. Tang, B. Shi, L. Gao, J.L. Daniels, H.T. Jiang, C. Liu, Urbanization effect on soil temperature in Nanjing, China, Energy Build. 43 (11) (2011) 3090–3098, https://doi.org/10.1016/j.enbuild.2011.08.003.
[62] S.S. Guo, C.Q. Zhu, N.S. Qiu, B.N. Tang, Y. Cui, J.T. Zhang, Y.H. Zhao, Present geothermal characteristics and influencing factors in the xiong'an new area, north China, Energies 12 (20) (2019), https://doi.org/10.3390/en12203884.
[63] Y.N. Sha, Analysis of geothermal anomaly distributing pattern and controlling factors in Southern Jiangsu (in Chinese), Coal Geolo.Chin. 20 (1) (2008) 34–36, https://doi.org/10.3969/j.issn.1674-1803.2008.01.012.
[64] V. Cermak, L. Bodri, M. Kresl, P. Dedecek, J. Safanda, Eleven years of ground-air temperature tracking over different land cover types, Int. J. Climatol. 37 (2) (2017) 1084–1099, https://doi.org/10.1002/joc.4764.
[65] H.T. Jiang, C.S. Tang, J.H. Wu, B. Shi, Effects of different covering pavement on subsurface soil temperature and moisture by long-term in-situ observation (in Chinese), J. Eng. Geol. 21 (6) (2013) 842–848, https://doi.org/10.3969/j.issn.1004-9665.2013.06.005.
[66] Z.Y. Qian, H.Y. Fu, Y. Wang, Y.T. Zhang, Characteristics of urban expansion and morphological evolution in Nanjing from 2004 to 2016 (in Chinese), Remote Sense Land Res. 31 (2) (2019) 149–156, https://doi.org/10.6046/gtzyyg.2019.02.21.
[67] B. Shi, C. Liu, W. Baojun, Z. Lizheng, Urban heat island effect on engineering properties of soil and the related disaster effect, Adv. Earth Sci. 23 (11) (2008) 1167–1173, https://doi.org/10.3321/j.issn:1001-8166.2008.11.007.